Bilayer sliding mechanism for the zinc-blende to rocksalt transition in SiC

Dorian M. Hatch,[1] Harold T. Stokes,[1] Jianjun Dong,[2] Jesse Gunter,[1] Hao Wang,[1] and James P. Lewis[1]
[1]*Department of Physics and Astronomy, Brigham Young University, Provo, Utah 84602, USA*
[2]*Physics Department, Auburn University, Auburn, Alabama 36849, USA*
(Received 14 September 2004; revised manuscript received 4 February 2005; published 25 May 2005)

We have theoretically investigated the mechanism of the pressure-induced reconstructive zinc-blende to rocksalt phase transition in SiC. We obtained 925 possible transition pathways (TPs) using a group-theoretical analysis method. This extensive survey of possible TPs is a significant feature which distinguishes this study from previous studies. Of these 925 TPs, we identified eight which have the lowest enthalpy barriers, based on first-principles electronic structure calculations. These eight TPs share a common underlying mechanism: bilayer sliding of (111) planes such that local bonding evolves from tetrahedral to octahedral without breaking any bonds. This mechanism may be applicable to other related transitions involving similar bonding changes.

DOI: 10.1103/PhysRevB.71.184109 PACS number(s): 64.70.Kb, 81.30.Kf, 05.70.Fh

I. INTRODUCTION

Silicon carbide (SiC) is of practical interest because of its use in novel electronic devices, abrasives, and refractories. It exhibits a wide band gap, a high breakdown field, low thermal expansion, oxidation resistance, excellent thermal shock resistance, and high thermal conductivity. In addition, it possesses favorable mechanical properties such as low density, high strength, high hardness, and high wear resistance. Changes in its structure, such as changes during a phase transition, can significantly alter these properties. X-ray-diffraction and shock experiments at high pressure[1–3] indicate a transition from the zinc-blende (ZB) to the rocksalt (RS) structure above 100 GPa in SiC. The coordination number of nearest neighbors changes from four to six during this transition. The transition is reversible and the zinc-blende structure is recovered below 35 GPa. Theoretical studies based on *ab initio* pseudopotential calculations[4–6] yield a transition pressure of 60 GPa and recent calculations using linear combination of atomic orbitals (LCAO) density functional theory (DFT) yield a value of 92 GPa.[7]

Increasing interest is being given to understanding the mechanism of a transition,[8–10] i.e., the changes which take place at the atomic level. Understanding the transition mechanism may lead to new experiments and measurements and possibly the control of transition properties. We take the mechanism for a phase transition to be the description of the displacements of all atoms along a transition path (TP). We assume periodicity is retained along the TP, the atoms throughout the crystal are displaced coherently (defects are neglected), and the crystal, as it moves from the initial to the final structure, defines a space group symmetry. Obtaining the transition mechanism is a challenging problem. Experimentally, Knudson and Gupta[9] reported a method where information from real-time picosecond time-resolved electronic spectroscopy coupled with *ab initio* calculations allowed the proposal of a TP in the wurtzite to rocksalt transition of CdS. Wickham *et al.*[10] showed that nanocrystal shape changes, as a function of pressure, determined by x-ray diffraction gave them details about the TP in the wurtzite to rocksalt transition in CdSe. On the theoretical side there are an infinite number of ways that one structure can be deformed into another. It is well known that diffusionless phase transitions, including reconstructive ones, with atomic displacements and shear can often be described by looking for a common subgroup of both structures.[11–14]

The ZB to RS transition in SiC has been widely studied. The first suggested transition path was based on a common subgroup with space group symmetry $R3m$.[6,15] Catti used LCAO-DFT methods to further investigate this TP and proposed an orthorhombic mechanism with a common subgroup symmetry of $Pmm2$ (Refs. 7,16) or more correctly $Imm2$.[17–19] He found that this TP was favored over the more simple TP of $R3m$. In another study of the transition mechanism, using sphere packing methods and no energy considerations, Sowa also obtained the $Imm2$ subgroup mechanism[20] and more recently proposed an additional mechanism with $P3_2$ symmetry.[21] Catti[16] and Sowa[20,21] have noted that in the $Imm2$ and P_32 TPs no silicon-carbon bonds are broken. However, no further study is reported on the comparison of the two TPs. The $Imm2$ TP is also contained in the unified path description of SiC polytypes transitions to rocksalt by Miao and Lambrecht.[22] The transition was also studied using conventional molecular dynamics (MD) simulation.[23] Making no assumptions about the atomistic mechanism, the SiC molecular dynamics cell evolved from cubic through a monoclinic cell at the equilibrium pressure. The monoclinic structure discovered in the MD simulation is similar to the RS structure in terms of local bonding. Presumably, the monoclinic structure is a metastable structure due to the fast-quenching artifact of MD simulations. No analysis of transition pathway was provided in the MD study.

We have developed a systematic procedure for obtaining possible microscopic mechanisms for reconstructive phase transitions and have applied it to the zinc-blende to rocksalt transitions in SiC. Some details of the algorithm are described by Stokes and Hatch[24,25] and has been used in our studies of the B1-to-B2 transition in sodium chloride and lead sulfide.[24–26] The procedure lets the user control the output by restricting allowed strain tolerance, nearest-neighbor distances, and unit-cell size change, and has been implemented in the computer program COMSUBS.[25] Using somewhat liberal input constraints, we obtained 925 possible atomistic TPs for this transition in SiC. This extensive survey of

possible TPs is a significant feature which distinguishes our current study from previous studies.

Calculation of enthalpy barriers for each of the 925 possible TPs imposes a challenge for conventional first-principles electronic structure calculations with plane wave basis. In this study, we adopted an efficient tight-binding based first-principles method called FIREBALL.[27] The FIREBALL results were verified with our plane wave calculations using the VASP method[28,29] for some selected TPs. The FIREBALL and VASP calculations are in close agreement, indicating that the general results presented in this paper are not sensitive to the first-principles computational methods adopted. In this paper, we discuss in detail our calculation of enthalpy along the TPs. An analysis of the enthalpy barriers for the TPs leads us to propose a *bilayer sliding* model to explain the mechanism of the ZB-to-RS transition. Such a model may be applicable to other related phase transitions involving similar tetrahedral-to-octahedral bonding changes.

II. ENERGETICALLY FAVORED PATHWAYS

First-principles calculations of the total energy in SiC were performed using FIREBALL.[27] This code is a density functional theory (DFT) [local density approximation (LDA), generalized gradient approximation, and spin polarization] approach to the electronic structure based on pseudopotentials and local orbitals; further details of the method can be found in Ref. 27. One of the important features of FIREBALL is the flexibility of constructing real-space localized basis functions to take advantage of fundamental chemistry in atomic bonding. This allows a substantial improvement in computational efficiency without suffering the loss of accuracy. Here we use the local density approximation (LDA) limit of DFT, the Harris functional[30] with a minimal nonorthogonal local-orbital basis of slightly excited orbitals.

The electronic eigenstates are expanded as a linear combination of pseudoatomic orbitals within a localized sp^3 basis for both carbon and silicon. These localized pseudoatomic orbitals, which we refer to as "fireballs," are slightly excited due to the boundary condition that they vanish at some radius $r_c(\psi^{\text{atomic}}_{\text{fireball}}(r)|_{r\geqslant r_c}=0)$ instead of the atomic boundary condition that they vanish at infinity. The cutoffs (4.5 and 5.4 Å for C and Si, respectively) are chosen in a way that preserves the relative ionization energies and relative atomic sizes for each species. The level of theory used is shown to be an accurate level of approximation for Si-C random alloys.[31]

We also performed some calculations using VASP, a first-principles DFT method, which is implemented with plane-wave basis sets,[28] ultrasoft pseudopotentials,[29] and LDA to the exchange-correlation interaction. The cutoff energy of the plane-wave bases is 287 eV. The integrations over the Brillouin zone were carried out by summing k points over Monkhorst-Pack grids. Careful tests have been done to ensure the numerical convergences for the k-point samplings and plane-wave cutoffs.

Using FIREBALL we calculated the lattice parameter a and the bulk modulus B for the SiC ZB structure at $P=0$, and obtained $a=4.46$ Å and $B=170$ GPa. The experimentally obtained values[32] are $a=4.31$ Å and $B=224$ GPa. We next calculated the phase transition pressure P_t at temperature $T=0$. This is simply the pressure at which the enthalpy $H=E+PV$ of the two phases are equal. We obtained $P_t=87$ GPa with $a=4.05$ Å in the ZB structure and $a=3.84$ Å in the RS structure. The experimentally obtained values[2] are $a=3.974$ Å and $a=3.684$ Å in the ZB and RS structures, respectively. Note that the transition displays a large amount of hysteresis ($P_t=100$ GPa for ZB$\rightarrow$RS and $P_t=35$ GPa for RS$\rightarrow$ZB). Our calculated value is consistent with the range resulting from the hysteresis. The transition pressure predicted by our VASP calculation is $P_t=64$ GPa, which is consistent with previous plane-wave results[6,15]

We used COMSUBS (Refs. 24,25) to find possible TPs from the ZB to the RS structure in SiC. (As the notes in Ref. 26 indicate, the algorithm described in Ref. 24 has undergone some major revisions.) We used relatively liberal constraints in the search. (1) We considered common subgroups with up to eight atoms per unit cell (four Si and four C). (2) We allowed principal values of the strain tensor to be between 0.6 and 1.6. (3) We allowed atoms to approach each other as close as 1.5 Å along straight-line TPs from the ZB to the RS structure. (4) We allowed atomic displacements as large as 2.0 Å.

With these constraints, we obtained 925 possible TPs for the transition. For each of these TPs, we used FIREBALL to estimate the enthalpy barrier by calculating the enthalpy along a linear TP. We varied each structural parameter (lattice parameters and atomic positions) according to

$$x_m = (1-\xi)x_{mi} + \xi x_{mf}, \tag{1}$$

where x_{mi} and x_{mf} are the initial and final values of the mth structural parameter x_m, and ξ is the "transition parameter" which varies from 0 to 1 as the transition takes place from the ZB to the RS structures. This obviously overestimates the true barrier height but provides an efficient way to determine

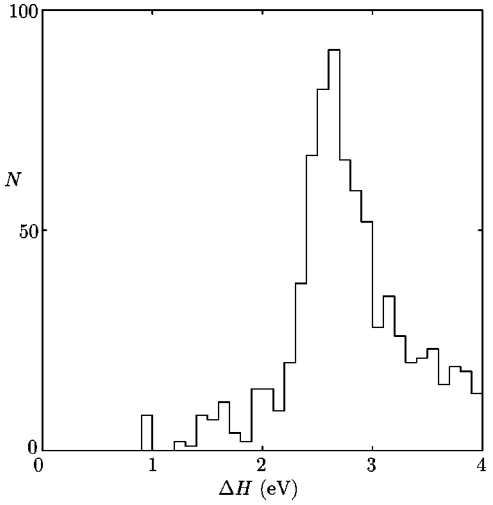

FIG. 1. Histogram of the enthalpy barrier heights ΔH_1 (per pair of atoms) for linear TPs between the ZB and RS structures.

TABLE I. Some possible TPs for the phase transition from the zincblende (ZB) to the rocksalt (RS) structure in SiC. Each TP is defined by a common subgroup G' of both ZB and RS. At each end of the transition, we give the lattice vectors of G' in terms of the lattice vectors of G and we give the atomic positions in the setting of G'. Note that for greater clarity we have changed many of the settings from those given in the output of COMSUBS.

TP	G'	G	Lattice	Si	C
1	44 *Imm*2	ZB	(0,−1/2,−1/2), (0,−1/2,1/2), (1, 0, 0)	(*a*) 0, 0, 0	(*b*) 0, 1/2, 1/4
		RS	(0,−1,0), (1/2,0,−1/2), (1/2,0,1/2)	(*a*) 0, 0, 0	(*b*) 0, 1/2, 1/2
2	9 *Cc*	ZB	(−1/2,−1/2,1), (1/2,−1/2,0), (1/2,1/2,1)	(*a*) 0, 1/4, 0	(*a*) −1/8, 1/4, 3/8
		RS	(1/2,1/2,−1), (−1/2,1/2,0), (1, 1, 0)	(*a*) 0, 1/2, 0	(*a*) 0, 0, 1/4
3	145 $P3_2$	ZB	(0,1/2,−1/2), (−1/2,0,1/2), (1, 1, 1)	(*a*) 1/3, 0, 0	(*a*) 1/3, 0, 3/4
		RS	(0,−1/2,1/2), (1/2,0,−1/2), (1, 1, 1)	(*a*) 0, −1/3, 0	(*a*) 2/3, 0, 5/6
4	1 *P*1	ZB	(1/2,−1/2,0), (1/2,0,−1/2), (1, 1, 1)	(*a*) 0, 0, 0	(*a*) 0, 0, 1/4
				(*a*) 2/3, 2/3, 1/3	(*a*) 2/3, 2/3, 7/12
				(*a*) 1/3, 1/3, 2/3	(*a*) 1/3, 1/3, 11/12
		RS	(1/2,0,−1/2), (0,1/2,−1/2), (1,1/2,3/2)	(*a*) 0, 0, 0	(*a*) 2/3, −1/6, 1/6
				(*a*) 4/3, 2/3, 1/3	(*a*) 1, 1/2, 1/2
				(*a*) 2/3, 1/3, 2/3	(*a*) 1/3, 1/6, 5/6
5	9 *Cc*	ZB	(1/2,−1,1/2), (1/2,0,−1/2), (3/2,1,3/2)	(*a*) 0, 1/4, 0	(*a*) −1/16, 1/4, 3/16
				(*a*) 3/4, 3/4, 1/4	(*a*) 11/16, 3/4, 7/16
		RS	(−1/2,1,−1/2), (−1/2,0,1/2), (1, 2, 1)	(*a*) 0, 1/2, 0	(*a*) 1/4, 1/2, 1/8
				(*a*) 1, 1, 1/4	(*a*) 3/4, 1/2, 3/8
6	9 *Cc*	ZB	(1/2,1/2,−1), (−1/2,1/2,0), (1, 1, 2)	(*a*) 0, 0, 0	(*a*) 5/8, 1/2, 3/16
				(*a*) 0, 1/2, 1/4	(*a*) 1/8, 1/2, 7/16
		RS	(−1/2,−1/2,1), (1/2,−1/2,0), (2, 2, 0)	(*a*) 0, 1/2, 0	(*a*) 1/2, 1/2, 1/8
				(*a*) 0, 1/2, 1/4	(*a*) 0, 0, 3/8
7	1 *P*1	ZB	(−1/2,1/2,0), (−1/2,0,1/2), (3/2,1,3/2)	(*a*) 0, 0, 0	(*a*) 1/8, 15/16, 3/16
				(*a*) 1/2, 1/4, 1/4	(*a*) 5/8, 3/16, 7/16
				(*a*) 0, 1/2, 1/2	(*a*) 1/8, 7/16, 11/16
				(*a*) 1/2, 3/4, 3/4	(*a*) 5/8, 11/16, 15/16
		RS	(1/2,−1/2,0), (1/2,0,−1/2), (1,5/2,1/2)	(*a*) 0, 0, 0	(*a*) −3/8, 9/8, 1/8
				(*a*) 1/4, 1/4, 1/4	(*a*) −1/8, 3/8, 3/8
				(*a*) −1/2, 1/2, 1/2	(*a*) −7/8, 5/8, 5/8
				(*a*) −1/4, 3/4, 3/4	(*a*) 3/8, 7/8, 7/8
8	1 *P*1	ZB	(−1/2,1/2,0), (−1/2,0,1/2), (3/2,1,3/2)	(*a*) 0, 0, 0	(*a*) 1/8, 15/16, 3/16
				(*a*) 1/2, 1/4, 1/4	(*a*) 5/8, 3/16, 7/16
				(*a*) 0, 1/2, 1/2	(*a*) 1/8, 7/16, 11/16
				(*a*) 1/2, 3/4, 3/4	(*a*) 5/8, 11/16, 15/16
		RS	(1/2,−1/2,0), (1/2,0,−1/2), (1, 2, 1)	(*a*) 0, 0, 0	(*a*) −1/2, 5/4, 1/8
				(*a*) 0, 1/2, 1/4	(*a*) −1/2, 3/4, 3/8
				(*a*) −1, 1, 1/2	(*a*) −1/2, 5/4, 5/8
				(*a*) 0, 3/2, 3/4	(*a*) 1/2, 3/4, 7/8
9	160 *R*3*m*	ZB	(−1/2,0,−1/2), (0,1/2,1/2), (1,1,−1)	(*a*) 0, 0, 0	(*a*) 0, 0, 3/4
		RS	(−1/2,1/2,0), (1/2,0,−1/2), (−1,−1,−1)	(*a*) 0, 0, 1/8	(*a*) 0, 0, 5/8
10	198 $P2_13$	ZB	(0,0,−1), (0,−1,0), (−1,0,0)	(*a*) 3/4, 3/4, 3/4	(*a*) 1/2, 1/2, 1/2
		RS	(−1,0,0), (0, 0, 1), (0, 1, 0)	(*a*) 1, 1, 1	(*a*) 1/2, 1/2, 1/2

which of the 925 TPs should be further considered as likely mechanisms for the phase transition.

In Fig. 1, we show a histogram of the enthalpy barrier heights obtained. The bar between 0.9 and 1.0 eV contains eight TPs. These TPs clearly stand alone as being most energetically favorable among the 925 TPs found by COMSUBS. The details about these eight TPs are given in Table I (TPs 1 through 8). The height of the enthalpy barrier along the linear TP is given in Table II (ΔH_1 column) and the barrier profiles are plotted in Fig. 2. (For completeness, two more TPs, 9 and 10, are added to the list in Table I. As noted earlier these additional TPs have been suggested in the lit-

TABLE II. Enthalpy barrier heights (eV per pair of atoms) for the TPs described in Table I. ΔH_1 is the barrier height for the linear TP. ΔH_2 is the barrier height for the TP using bow functions, but constrained by the symmetry of the common subgroup G' listed in Table I. $\Delta H_{2,VASP}$ are these same barrier heights calculated using VASP. ΔH_3 is the barrier height for TP using additional bow functions, constrained by the symmetry of the common subgroup G' listed in Table IV. N_1 is the number of atoms per unit cell used for the calculation of ΔH_1 and ΔH_2. N_3 is the number of atoms per unit cell used for the calculation of ΔH_3. N_w is the number of structural parameters (and the number of new function weights) used for the calculation of ΔH_2 for TPs 4, 7, 8 and ΔH_3 for the other TPs.

TP	ΔH_1	ΔH_2	$\Delta H_{2,\mathrm{VASP}}$	ΔH_3	N_1	N_3	N_w
1	0.97	0.62	0.61	0.52	2	8	18
2	0.91	0.65	0.69	0.52	4	8	27
3	0.97	0.69	0.57	0.54	6	6	21
4	0.92	0.51			6		21
5	0.94	0.67		0.53	8	8	27
6	0.95	0.57		0.54	8	8	27
7	0.96	0.54			8		27
8	0.98	0.51			8		27
9	1.99	1.68	1.86	1.39	2	8	27
10	3.78	3.01		1.99	8	8	27

erature, but are not energetically favorable according to our calculations.)

We now consider in more detail TPs 1 through 8. Previous theoretical studies of structural phase transitions have primarily considered only high-symmetry TPs with a small number of structural parameters. In contrast, our current study includes low-symmetry TPs with a large number of structural parameters and therefore imposes computational challenges for finding how the structural parameters vary along the true TP.

We have developed an efficient numerical algorithm (called the bow-function method) for finding an approximation to the TP by locating the point which occurs at the highest value along the true TP. This point is a saddle point with respect to the structural parameters. We assume that the linear TP in Eq. (1) is already a reasonable initial estimation of the true TP. We also assume that the peak on the linear TP is not too far distant from the saddle point on the true TP. The problem at hand is how to get from the peak in the linear TP to the saddle point in the true TP. If we simply minimize the enthalpy with respect to the structural parameters, we will "fall off" the saddle point. We solve this problem by adding a quadratic term (called a bow function) to the linear TP:

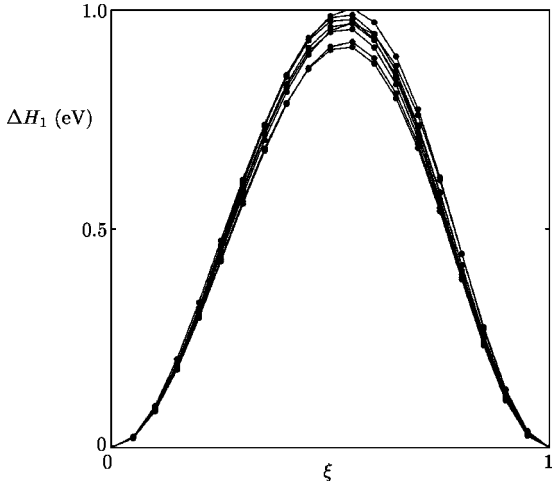

FIG. 2. Enthalpy barriers ΔH_1 as a function of the transition parameter ξ along each of the first eight TPs described in Table I. The TPs are linear with no bow-function corrections.

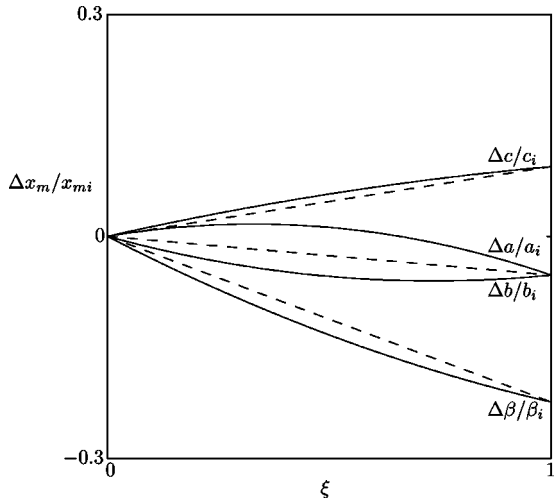

FIG. 3. Fractional change in monoclinic lattice parameters ($x_m = a, b, c, \beta$) as a function of the transition parameter ξ along TP 2. Dashed lines show the linear TPs, and solid lines show the TPs with the bow-function corrections (but still maintaining the symmetry of $G' = Cc$).

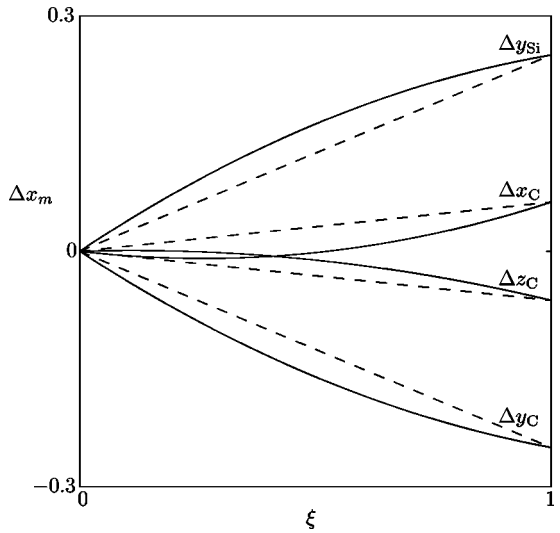

FIG. 4. Change in dimensionless atomic positions ($x_m = y_{\mathrm{Si}}, x_{\mathrm{C}}, y_{\mathrm{C}}, z_{\mathrm{C}}$) as a function of the transition parameter ξ along TP 2. Dashed lines show the linear TPs, and solid lines show the TPs with the bow-function corrections (but still maintaining the symmetry of $G' = Cc$).

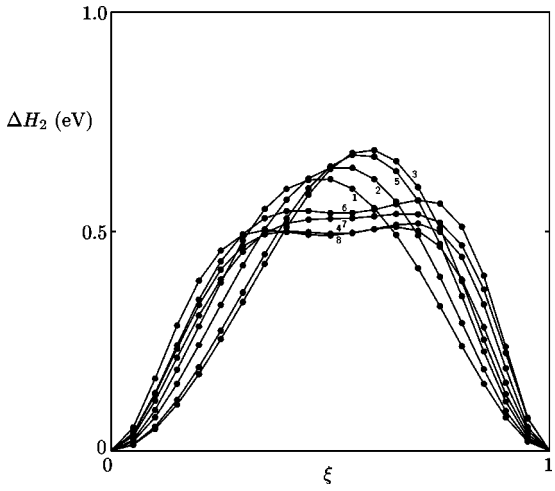

FIG. 5. Enthalpy barriers ΔH_2 as a function of the transition parameter ξ along each of the first eight TPs described in Table I. The TPs include bow-function corrections that maintain the symmetry given in Table I.

$$x_m = (1-\xi)x_{mi} + \xi x_{mf} + w_m \xi(1-\xi), \tag{2}$$

where w_m is the "weight" of the bow function for the mth structural parameter x_m. (Similar bow functions were used in Ref. 26.) We find the saddle point on the true TP by minimizing the height of the peak on the TP with respect to the weights w_m.

The minimization algorithm is straightforward. We begin with the linear TP where all of the weights w_m are zero. We locate the enthalpy peak, which is usually near $\xi=0.5$. We then change one of the weights in either a positive or negative direction. This may move the position of the peak, so we locate the peak again. (As will be seen, some of our TPs exhibit two peaks, so we always search for the highest peak across the entire TP, not just in the vicinity of the location of the peak before we changed the weight.) Then we check if the height of the peak is lower than before we changed the weight. If so, we keep the change. If not, we undo the change. We repeat this for each of the weights until we finally arrive at the situation where no positive or negative

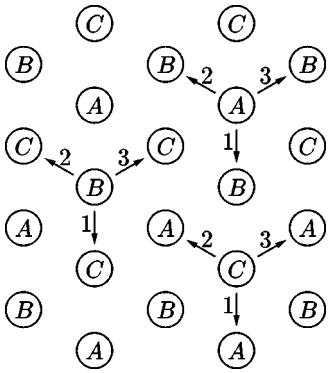

FIG. 6. Projection of an fcc lattice onto the cubic (111) plane. Arrows show sliding directions which change A planes into B planes, B planes into C planes, and C planes into A planes.

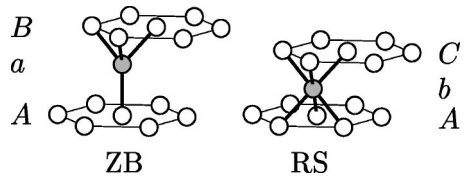

FIG. 7. (111) planes of atoms in the ZB and RS structures. The open circles represent Si atoms, and the filled circles represent C atoms. In the transition from ZB to RS, the top two planes slide with respect to the bottom plane.

change in any weight lowers the height of the peak. This final point at the top of the peak is the saddle point. The enthalpy increases with respect to changes in all of the variables (the weights) except one (the transition parameter ξ).

Even though the TP we obtain is approximate it passes through the saddle point on the true TP, and we thus obtain the barrier height of the true TP. Our TP matches the true TP at three points: the end points and the saddle point at the top of the barrier and is a smooth quadratic curve which passes through those three points.

The success of the bow-function method depends on an enthalpy landscape which is smooth and simple. It would fail to find the true saddle point if, for example, the true TP followed twisting "canyons" so that the saddle point at the top of the barrier is enclosed by higher peaks and inaccessible to the bow functions. Even if the true saddle point is found, a complex enthalpy landscape could cause the true TP to have important features which would be missed by our approximate TP.

These are concerns in our present work because our final TPs, as will be seen, do not exhibit a simple single peak. It appears that the landscape could be quite complex, and our bow-function method may not have found the true saddle points. In that case, our enthalpy barrier heights would be an overestimation of the true barrier heights. Furthermore, our approximate TPs might even miss features of the true TPs which are important for the understanding of the transition mechanism. Because of the large number of dimensions in the configuration space (one dimension for each structural parameter), it is not even possible, with current computer technology, to investigate the enthalpy landscape in sufficient detail to determine how good our approximate TPs are.

This being said, we nevertheless have confidence that in our present work, the bow-function method produces TPs which have all of the essential features of the true TPs. As will be seen, the TPs we obtained have helped us discover a bilayer sliding mechanism common to all eight TPs with the

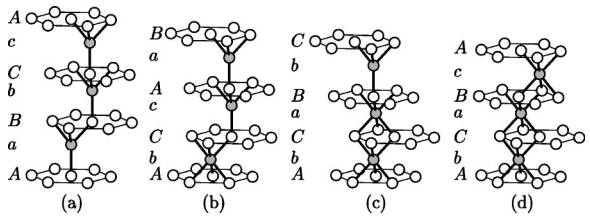

FIG. 8. A sequence of bilayer slidings that takes the ZB structure in (a) to the RS structure in (d).

TABLE III. For each TP, the sequence of slidings of adjacent bilayers is given. The numbers in the sequences refer to directions indicated in Fig. 7. Also, the shear strain ϵ is given for each TP.

TP	Sequence	ϵ
1	1	0.71
2	12	0.35
3	123	0.0
4	112	0.41
5	1213	0.18
6	1122	0.35
7	1112	0.47
8	1123	0.18

lowest barriers. Furthermore, it is only with the help of these TPs that we could have discovered how the barrier height is lowered by allowing different bilayers to slide at different rates. When a large number of structural parameters are present, the bow-function method is a powerful tool for investigating TPs in reconstructive phase transitions.

As an example, consider TP 2 listed in Table I. For the linear TP, the barrier height is 0.91 eV per pair of atoms (ΔH_1 in Table II). The symmetry of the crystal along this linear TP is monoclinic, space group No. 9 *Cc*. Both the Si and C atoms are at the Wyckoff (a) position x, y, z. There are eight structural parameters: the monoclinic lattice parameters a, b, c, β and the atomic positions $y_{\mathrm{Si}}, x_{\mathrm{C}}, y_{\mathrm{C}}, z_{\mathrm{C}}$. (Since the x and z components of the origin of *Cc* are arbitrary, we hold x_{Si} and z_{Si} fixed.) When we minimize the barrier height with respect to the eight weights w_m, we obtain 0.65 eV per pair of atoms (ΔH_2 in Table II), a considerable improvement over the linear TP. In Fig. 3, we show the fractional change in the lattice parameters a, b, c, β as a function of the transition parameter ξ. The dashed lines show the changes for the linear TP given by Eq. (1). The solid lines show the changes which include the bow functions, as in Eq. (2). In Fig. 4, we show the changes in the atomic positions.

In Fig. 5, we plot the enthalpy barrier ΔH_2 for TPs 1 through 8. Each barrier height has been minimized using bow functions. The values for ΔH_2 are given in Table II. For TPs 1,2,3,9, we obtained similar results using VASP, as can be seen in the table. The plane-wave VASP method is much more computationally demanding than the local basis FIREBALL method. Our motivation for adopting a local basis method here is because of its efficiency. By sacrificing a minor reduction in the accuracy, we can achieve a significant improvement on computational efficiency with our optimized basis sets. It was not deemed practical to calculate any of the other barrier heights using VASP. As shown in Table II, results from the two computational methods are in good agreement for the selected TPs and both methods provided a consistent picture of which TPs have low barriers, relative to the others, and thus which are the favored pathways.

It is worth noting that the two previously suggested low-barrier *Imm*2 and $P_3 2$ TPs are included in our eight favorable TPs found in this study. Our study also agrees with the previous study that both $R3m$ and $P2_13$ TPs have noticeably higher transition barriers, which makes them less favorable.

III. TRANSITION MECHANISM

An analysis of the eight most favored TPs shows that they share one common feature, i.e., they correspond to the eight possible ways that atomic bilayers in (111) cubic planes slide relative to one another with no broken bonds, if we allow repeat units up to four bilayers. Our bilayer sliding model is best illustrated by projecting the face-centered cubic (fcc) lattice onto the (111) plane (see Fig. 6). The positions marked A, B, C lie in different (111) planes. These planes are stacked with the repeating sequence *ABCABC*… (or, equivalently, *ACBACB*…). If we place the silicon atoms at the lattice points, then the carbon atoms lie in planes between the silicon planes. We denote the silicon positions with A, B, C and the carbon positions with a, b, c. [The A and a planes project onto identical points on the (111) plane. We just use upper and lower case letters to distinguish between Si and C planes.] Using this notation, the repeat unit of stacking in ZB is *AaBbCc* (or *AaCcBb*) and in RS is *AcBaCb* (or *AbCaBc*).

In Fig. 7, we show how the (111) planes slide to change a ZB structure into a RS structure without breaking any bonds. In ZB, the carbon atoms of one plane sit directly above the silicon atoms in the plane below (the a and A planes shown in the figure). There is one bond between each carbon atom and the silicon atom in the plane below. The carbon atoms also sit directly below a "pocket" of silicon atoms in the plane above (the a and B planes of the figure). Each carbon atom is bonded to three silicon atoms in that plane. This is a total of four bonds per carbon atom in ZB. To change from ZB to RS, the *aB* bilayer slides so that the C atom now sits in a pocket of silicon atoms of the plane below. This sliding causes the *aB* bilayer to become a *bC* bilayer. Each carbon atom is now bonded to three silicon atoms in the plane below as well as in the plane above, a total of six bonds. The four silicon atoms to which each carbon atom is bonded in ZB remain bonded to that carbon atom in RS. The sliding causes two more silicon atoms to be bonded to each carbon atom, raising the number of bonds from four to six. This is what we mean by "no broken bonds."

As shown in Fig. 8, the first-step sliding between the A and *aB* layers changes the stacking sequence from *AaBbCcAaBbCc* [Fig. 8(a)] to *AbCcAaBbCcAa* [Fig. 8(b)]. Note that every layer above the *aB* bilayer is shifted along with the *aB* bilayer, leading to a relabeling of every subsequent layer. Next, we slide the *cA* bilayer with respect to the C layer below it, and we obtain *AbCaBbCcAaBb* [Fig. 8(c)]. And finally, we slide the *bC* bilayer with respect to the B layer, and we obtain *AbCaBcAaBbCc* [Fig. 8(d)]. We now have one repeat unit of the RS structure: *AbCaBc*. We repeat this procedure to change each repeat unit of ZB into a repeat unit of RS. Of course, in an actual phase transition, all of these slidings take place simultaneously.

The eight favorable TPs differ in the combination of the sliding directions in the bilayer sliding sequence. As can be seen, we require slidings that change A into B layers, B into C layers, and C into A layers. From Fig. 6, we see that for

TABLE IV. TPs from Table I with the symmetry lowered so that the motion of each cubic (111) plane within the unit cell is independent along the TP.

TP	G'	G	Lattice	Si	C
1	8 *Cm*	ZB	(1,−1/2,−1/2), (0,−1/2,1/2), (2, 1, 1)	(*a*) 0, 0, 0	(*a*) 5/8, 0, 1/16
				(*a*) 1/2, 0, 1/4	(*a*) 1/8, 0, 5/16
				(*a*) 0, 0, 1/2	(*a*) 5/8, 0, 9/16
				(*a*) 1/2, 0, 3/4	(*a*) 1/8, 0, 13/16
		RS	(1/2,−1,1/2), (1/2,0,−1/2), (1, 2, 1)	(*a*) 0, 0, 0	(*a*) 3/4, 0, 1/8
				(*a*) 1/2, 0, 1/4	(*a*) 1/4, 0, 3/8
				(*a*) 0, 0, 1/2	(*a*) 3/4, 0, 5/8
				(*a*) 1/2, 0, 3/4	(*a*) 1/4, 0, 7/8
2	1 *P*1	ZB	(0,−1/2,1/2), (1/2,0,−1/2), (1, 1, 2)	(*a*) 0, 0, 0	(*a*) 7/8, 1/8, 3/16
				(*a*) 1/2, 1/2, 1/4	(*a*) 3/8, 5/8, 7/16
				(*a*) 0, 0, 1/2	(*a*) 7/8, 1/8, 11/16
				(*a*) 1/2, 1/2, 3/4	(*a*) 3/8, 5/8, 15/16
		RS	(0,1/2,−1/2), (−1/2,0,1/2), (2, 2, 0)	(*a*) 0, 0, 0	(*a*) −1/2, 1/2, 1/8
				(*a*) 0, 0, 1/4	(*a*) 1/2, 1/2, 3/8
				(*a*) 0, 0, 1/2	(*a*) −1/2, 1/2, 5/8
				(*a*) 0, 0, 3/4	(*a*) 1/2, 1/2, 7/8
3	1 *P*1	ZB	(0,1/2,−1/2), (−1/2,0,1/2), (1, 1, 1)	(*a*) 0, 0, 0	(*a*) 1/3, 2/3, 1/12
				(*a*) 1/3, 2/3, 1/3	(*a*) 2/3, 1/3, 5/12
				(*a*) 2/3, 1/3, 2/3	(*a*) 0, 0, 3/4
		RS	(0,−1/2,1/2), (1/2,0,−1/2), (1, 1, 1)	(*a*) 0, 0, 0	(*a*) 1/3, 2/3, 1/6
				(*a*) 2/3, 4/3, 1/3	(*a*) 1, 1, 1/2
				(*a*) 4/3, 2/3, 2/3	(*a*) 2/3, 1/3, 5/6
5	1 *P*1	ZB	(1/2,−1/2,0), (0,1/2,−1/2), (3/2,1,3/2)	(*a*) 0, 0, 0	(*a*) −1/16, 1/16, 3/16
				(*a*) 1/4, 3/4, 1/4	(*a*) 3/16, 13/16, 7/16
				(*a*) 1/2, 1/2, 1/2	(*a*) 7/16, 9/16, 11/16
				(*a*) 3/4, 1/4, 3/4	(*a*) 11/16, 5/16, 15/16
		RS	(−1/2,1/2,0), (0,−1/2,1/2), (1, 2, 1)	(*a*) 0, 0, 0	(*a*) 1/4, −1/4, 1/8
				(*a*) 1/2, 1/2, 1/4	(*a*) −1/4, 1/4, 3/8
				(*a*) 0, 0, 1/2	(*a*) 1/4, −1/4, 5/8
				(*a*) 1/2, −1/2, 3/4	(*a*) 3/4, 1/4, 7/8
6	1 *P*1	ZB	(0,1/2,−1/2), (−1/2,0,1/2), (1, 1, 2)	(*a*) 0, 0, 0	(*a*) 1/8, 7/8, 3/16
				(*a*) 1/2, 1/2, 1/4	(*a*) 5/8, 3/8, 7/16
				(*a*) 0, 0, 1/2	(*a*) 1/8, 7/8, 11/16
				(*a*) 1/2, 1/2, 3/4	(*a*) 5/8, 3/8, 15/16
		RS	(0,−1/2,1/2), (1/2,0,−1/2), (2, 2, 0)	(*a*) 0, 0, 0	(*a*) −1/2, 1/2, 1/8
				(*a*) 0, 0, 1/4	(*a*) −1/2, −1/2, 3/8
				(*a*) −1, −1, 1/2	(*a*) −1/2, 1/2, 5/8
				(*a*) 0, 0, 3/4	(*a*) 1/2, 1/2, 7/8

each case, the slide can take place in three different directions which we label 1,2,3. The intermediate structures along the TPs from ZB to RS are distinguished by the relative directions of the slidings. For example, we obtain TP 1 when we slide every bilayer in the same direction. Every bilayer is equivalent along this TP, leading to a structure with the same size of primitive unit cell as in ZB and RS. We obtain TP 2 when we slide alternate bilayers along directions 1 and 2, respectively. This leads to a structure with a primitive unit cell twice as large as that in ZB and RS. The sliding sequence in Fig. 8 actually depicts TP 3 where the three slidings shown are in directions 1,2,3, respectively.

In Table III, we show the repeat unit of the sequence of sliding directions for TPs 1 through 8. This table gives every unique way in which this sliding can take place for repeat units up to four bilayers. Based on this analysis, we can draw an important conclusion that COMSUBS *has found every possible way this can be done* for the sequences of sliding direction which have repeating units of up to four. Additional TPs can be found if longer repeating units are allowed. How-

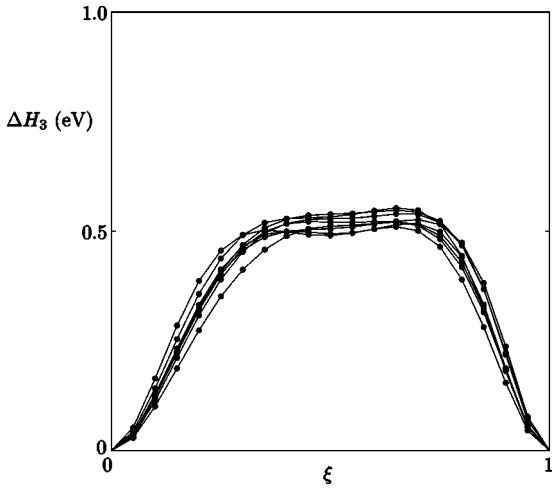

FIG. 9. Enthalpy barriers ΔH_3 as a function of the transition parameter ξ along each of the first eight TPs described in Table I. The TPs include bow-function corrections that maintain the symmetry given in Table I for TPs 4,7,8 and the symmetry given in Table IV for TPs 1,2,3,5,6.

ever, those TPs are expected to have similar barrier heights as the eight TPs listed here.

Now we return to the barriers shown in Fig. 5. We note that four of the TPs (4,6,7,8) have barrier heights that are substantially lower than the others and appear to be a superposition of two or more peaks. Three of them (TPs 4,7,8) have the triclinic symmetry, space group No. 1, *P*1. Each atom in the unit cell belongs to a different (111) layer. This allows the (111) bilayers in the unit cell to move *independent* of each other. We see in Fig. 2 that the peak of the barrier occurs when adjacent bilayers have slid about half way ($\xi \approx 0.5$). If some adjacent bilayers could slide ahead of others, then the peak in the barrier for different adjacent bilayers would be crossed at different values of ξ. This could lead to an overall lower barrier with a shape that would appear to be a superposition of two or more peaks. (We note that TP 6 also shows this feature, even though the space-group symmetry *Cc* does not allow the motion of all four planes to be independent of each other. In this case, the symmetry still allows the peaks to be crossed at different values of ξ.) This suggests that if we lowered the symmetry of the other TPs so that there are three or more inequivalent (111) bilayers in the unit cell, we can lower the barrier heights of the other TPs as well. (Note that this does not agree with the conjecture that transitions will follow paths with maximal subgroup symmetry.)

In Table IV we give the new settings required for TPs 1,2,3,5,6. In these new settings, the number of structural parameters and associated bow functions are greatly increased. For example, in a triclinic unit cell containing eight atoms, there are 27 structural parameters. Minimizing the enthalpy barrier with respect to 27 weights would be possible only for a highly efficient computational method such as FIREBALL.

In Fig. 9, we plot the enthalpy barriers ΔH_3 we obtain using the increased number of bow functions allowed by the lower symmetry. We also include from Fig. 5 the barriers for TPs 4,7,8. As can be seen, the barrier heights and shapes are nearly the same for every TP. In Table II, we give the numerical values ΔH_3 for these barrier heights. Note that the lower symmetry in TP 6 had very little effect on the barrier height and shape.

On the basis of Fig. 9, we conclude that all eight TPs are equally energetically favorable, to within the accuracy of FIREBALL. However, the strain accompanying a transition must also be considered. We assume in our calculations that the entire crystal transforms coherently. In reality, phase transitions generally result in a number of domains with different orientations. A large anisotropic strain can hinder a phase transition as different domains try to strain the crystal in different directions. In the present case, the sliding of the cubic (111) planes causes a shear strain. Using the sequences in Table III and the directions in Fig. 6, the shear strain for each TP can be easily calculated. We give the results in Table III.

For example, in TP 1, every (111) bilayer slides a distance $a/\sqrt{6}$ (a is the lattice parameter of the cubic unit cell) relative to the adjacent bilayer. The (111) bilayers are a distance $a/\sqrt{3}$ apart. This results in a shear strain of $(a/\sqrt{6})/(a/\sqrt{3}) = 1/\sqrt{2}$.

In TP 2, alternating (111) bilayers are displaced in directions 1 and 2, respectively. If we add these two directions, we obtain a net displacement of the same amount $a/\sqrt{6}$ but in a direction opposite to direction 3. This displacement occurs over two bilayers, so the shear strain is $(a/\sqrt{6})/(2a/\sqrt{3}) = 1/2\sqrt{2}$.

In TP 3, the sum of displacements in directions 1,2,3 is zero, resulting in zero shear strain. In fact, this is the only TP among the eight that has zero shear strain. This favors TP 3 over the others.

IV. CONCLUSION

In summary, we have systematically studied the possible transformation pathways for the zinc-blende to rocksalt transition in SiC with the cell sizes of intermediate structures up to eight atoms. Our first-principles calculations have identified eight favorable TPs among the 925 possible candidates listed by a COMSUBS analysis. Common features in the eight favorable TPs leads us to the discovery of the bilayer sliding mechanism for the structural transformation of this type. According to this model, all the related TPs (even when longer repeating sequences are considered) are equally favorable in terms of enthalpy barrier heights. The only thing we can really conclude is that the transition takes place by some sequence of (111) bilayer slidings. In a real sample, the sequence of sliding directions may even be random without a definite period. However, we would expect all three directions to be present in approximately equal amounts so that a minimal amount of shear strain would occur.

ACKNOWLEDGMENTS

We acknowledge financial support from the U.S. Department of Energy under Contract No. DE-FG02-03ER46059 and No. DE-FG02-03ER46060.

[1] K. Stössner and M. Cardona, Solid State Commun. **63**, 1113 (1987).
[2] M. Yoshida, A. Onodera, M. Ueno, K. Takemura, and O. Shimomura, Phys. Rev. B **48**, 10 587 (1993).
[3] T. Sekine and T. Kobayashi, Phys. Rev. B **55**, 8034 (1997).
[4] N. E. Christensen, S. Satpathy, and Z. Pawlowska,, Phys. Rev. B **36**, 1032 (1987).
[5] K. J. Chang and M. L. Cohen, Phys. Rev. B **35**, 8196 (1987).
[6] K. Karch, F. Bechstedt, P. Pavone, and D. Strauch, Phys. Rev. B **53**, 13 400 (1996).
[7] M. Catti, Phys. Rev. Lett. **87**, 035504 (2001).
[8] *Shock Compression of Condensed Matter-1991*, edited by S. C. Schmidt, R. D. Dick, J. W. Forbes, and D. G. Tasker (Elsevier Science, Amsterdam, 1992).
[9] M. D. Knudson, Y M. Gupta, and A. B. Kunz, Phys. Rev. B **59**, 11 704 (1999).
[10] J. N. Wickham, A. B. Herhold, and A. P. Alivisatos, Phys. Rev. Lett. **84**, 923 (2000).
[11] V. P Dmitriev, S. B. Rochal, Yu. M. Gufan, and P. Toledano, Phys. Rev. Lett. **60**, 1958 (1988).
[12] C. Mailhiot and A. K. McMahan, Phys. Rev. B **44**, 11 578 (1991).
[13] A. G. Christy, Acta Crystallogr., Sect. B: Struct. Sci. **49**, 987 (1993).
[14] M. O'Keeffe and B. G. Hyde, *Crystal Structures I. Patterns and Symmetry* (Mineralogical Society of America, Washington, 1996).
[15] M. A. Blanco, J. M. Recio, A. Costales, and R. Pandey, Phys. Rev. B **62**, R10 599 (2000).
[16] M. Catti, Phys. Rev. B **65**, 224115 (2002).
[17] M. S. Miao, M. Prikhodko, and W. R. L. Lambrecht, Phys. Rev. B **66**, 064107 (2002).
[18] M. S. Miao, M. Prikhodko, and W. R. L. Lambrecht, Phys. Rev. Lett. **88**, 189601 (2002).
[19] J. M. Perez-Mato, M. Aroyo, C. Capillas, P. Blaha, and K. Schwarz, Phys. Rev. Lett. **90**, 049603 (2003).
[20] H. Sowa, Z. Kristallogr. **215**, 335 (2000).
[21] H. Sowa, Acta Crystallogr., Sect. A: Found. Crystallogr. **59**, 266 (2003).
[22] M. S. Miao and W. R. L Lambrecht, Phys. Rev. B **68**, 092103 (2003).
[23] F. Shimojo, I Ebbsjo, R. K. Kalia, A. Nakano, J. P Rino, and P. Vashishta, Phys. Rev. Lett. **84**, 3338 (2000).
[24] H. T. Stokes and D. M. Hatch, Phys. Rev. B **65**, 144114 (2002).
[25] H. T. Stokes and D. M. Hatch, Isotropy Software Package, http://stokes.byu.edu/isotropy.html, 2004.
[26] H. T. Stokes, D. M. Hatch, J. Dong, and J. P. Lewis, Phys. Rev. B **69**, 174111 (2004).
[27] J. P. Lewis, K. R. Glaesemann, G. A. Voth, J. Fritsch, A. A. Demkov, J. Ortega, and O. F. Sankey, Phys. Rev. B **64**, 195103 (2001).
[28] G. Kresse and J. Hafner, Phys. Rev. B **47**, R558 (1993); G. Kresse and J. Furthmuller, Comput. Mater. Sci. **6**, 15 (1996).
[29] D. Vanderbilt, Phys. Rev. B **41**, R7892 (1990); G. Kresse and J. Hafner, J. Phys.: Condens. Matter **6**, 8245 (1994)
[30] J. Harris, Phys. Rev. B **31**, 1770 (1985).
[31] A. A. Demkov and O. F. Sankey, Phys. Rev. B **48**, 2207 (1993).
[32] N. Churcher, K. Kunc, and V. Heine, J. Phys. C **19**, 4413 (1986).